Journal Pre-proof

High Performance Quantum Piezotronic Tunneling Transistor based on Edge States of MoS_2 Nanoribbon

Minjiang Dan, Gongwei Hu, Lijie Li, Yan Zhang

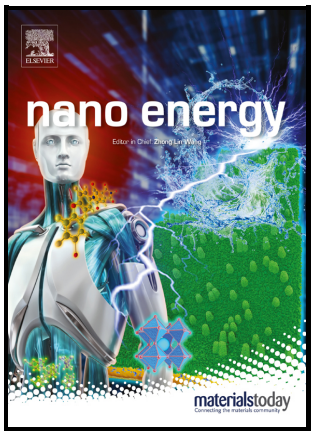

PII: S2211-2855(22)00354-8

DOI: https://doi.org/10.1016/j.nanoen.2022.107275

Reference: NANOEN107275

To appear in: *Nano Energy*

Received date: 5 March 2022
Revised date: 4 April 2022
Accepted date: 10 April 2022

Please cite this article as: Minjiang Dan, Gongwei Hu, Lijie Li and Yan Zhang, High Performance Quantum Piezotronic Tunneling Transistor based on Edge States of MoS_2 Nanoribbon, *Nano Energy,* (2022) doi:https://doi.org/10.1016/j.nanoen.2022.107275

High Performance Quantum Piezotronic Tunneling Transistor based on Edge States of MoS_2 Nanoribbon

Minjiang Dan[1], Gongwei Hu[1], Lijie Li[2,*] and Yan Zhang[1,3,4,*]

[1] School of Physics, University of Electronic Science and Technology of China, Chengdu 610054, China

[2] College of Engineering, Swansea University, Swansea, SA1 8EN, UK

[3] Beijing Institute of Nanoenergy and Nanosystems, Chinese Academy of Sciences; Beijing 100083, China

[4] College of Nanoscience and Technology, University of Chinese Academy of Sciences, Beijing 100049, China

[*]To whom correspondence should be addressed, E-mail: zhangyan@uestc.edu.cn and L.Li@swansea.ac.uk

Abstract

High performance edge states-based quantum piezotronic tunneling transistor with MoS_2 nanoribbon device architecture at room temperature is demonstrated. The edge states are identified by the tight-binding band calculations. The Fermi energy position related to carrier concentration and tunneling probability are investigated based on quantum mechanics theory. It is found that the tunneling current can be exponentially controlled by piezotronic effect, and the Schottky barrier height can also be modified. The edge states transport behavior is further elucidated by conductance and electronic density distribution with applied strains. The strain sensitivity of the quantum piezotronic transistor can reach over 10^3. This study is capable of advancing the design of new generation of transistor devices based on edge states, and providing prospects of realizing high performance room temperature quantum piezotronic devices.

Keywords: edge states, MoS_2 nanoribbon, piezotronic effect, quantum tunneling transistor

1. Introduction

Piezotronics has been attracting tremendous research interests dur to their unique two-way coupling of piezotronic effect and semiconductor properties. Strain-induced piezoelectric polarization charges at the junction can effectively control the carrier generation, transport, and recombination process [1-3]. Benefiting from the mechanism, many high performance piezotronics devices have been innovatively developed, such as nanogenerators [4-6], strain sensors [7], piezoelectric field-effect transistors [8], addressable transistor arrays [9] and piezotronic logic nanodevices [10, 11]. Piezotronic and piezo-phototronic devices have high performances because strain-induced polarization controls Schottky barrier heights [1, 2, 12]. Typical ZnO nanowire-based piezotronic strain sensor has gauge factor of 1250 by the piezotronic effect [7]. Recently, ultrahigh sensitivity of strain sensors based on piezotronic Ag/HfO_2/n-ZnO junction reached up to 4.8×10^5 gauge factor at 0.10% strain, because strain-induced polarization controls the metal/insulator/piezoelectric semiconductor structure [13]. Piezotronic effect is effectively exploited to develop oxygen [14], glucose [15], protein [16] and humidity [17] sensors based on strain-controlled Schottky barrier.

Piezotronic and piezo-phototronic transistors can be good candidates for high performance quantum devices. Room-temperature quantum devices face great challenge for quantum communication and computation [18-20]. Piezo-phototronic spin lasers operated at room temperature have been studied theoretically and experimentally [21-23]. Edge states, as a novel feature of transition metal dichalcogenide (TMDC), holds enormous potential towards future high performance electronic applications at room temperature. The edge states of MoS_2 nanoparticles and nanoclusters have been directly observed by atom-resolved scanning tunneling microscopy at room temperature [24, 25]. Theoretical analysis has identified that the insulating or metallic edge states can be stable according to the temperature and ambience [26]. Furthermore, edge states can be utilized to realize the topological superconducting phases and search for Majorana zero modes [27, 28]. Most importantly, composite wide-band saturable absorbers and field-effect transistors have been fabricated based on the edge states in layered MoS_2 [29, 30]. Two-dimensional layered TMDC materials have been outstanding options for transistor application in the research community because of their atomically thin planar structure, finite band gap, ease of fabrication, excellent flexibility and electrostatic

controllability [31-36]. Abundant effort has been contributed to develop electronic devices based on the quantum mechanical transportation, such as band to band tunneling (BTBT) [37, 38] and Schottky barrier tunneling [39, 40].

In this study, we have constructively designed high performance monolayer armchair MoS_2 nanoribbon-based quantum tunneling transistor to utilize the edge states transport at room temperature. The influence of strain-induced piezotronic effect on barrier potential and Schottky barrier height has been discussed in detail. The existence of edge states can be explicitly observed in the band structure through tight-binding model. In order to calculate the tunneling current, we have also investigated the carrier concentration-related Fermi energy and quantum mechanical tunneling probability. The tunneling current change under strain, temperature and carrier concentration has been studied systematically. Strain reveals an exponential control with ultrahigh sensitivity over 10^3 which is also verified by the conductance and electronic density distribution of edge states transport. These results not only open up instructive design guidance for electronic devices based on edge states, but also provide innovative ideas for high performance piezotronics device at room temperature.

2. Model and method

TMDC monolayers are intrinsically piezoelectric materials due to the lack of centrosymmetry [41]. When an external strain s is applied in the armchair direction, the strain-induced polarization can be expressed as $P = e_{11}s$, where e_{11} is the piezoelectric coefficient of monolayer MoS_2 [42]. The source side is set to be ohmic contact, then there only exists piezoelectric polarization charges at the drain side. The strain-induced piezoelectric potential distribution can be approximately obtained through 1D infinite charged wire model [43-45]

$$V_{piezo} = \frac{P}{2\pi\varepsilon_0\varepsilon_r}\ln\left(\frac{L-x}{L}\right) \tag{1}$$

where L is the nanoribbon length, ε_0 and ε_r are the vacuum and relative dielectric constants, respectively, x is the distance along the armchair direction away from Mo-terminated edge.

The electronic structure and edge states dispersion properties can be well characterized by employing the tight-binding model. The tight-binding Hamiltonian reads as follows [46, 47]

$$H^{TB} = \sum_{i,\mu\nu} \epsilon_{\mu,\nu} c_{i,\mu}^{\dagger} c_{i,\nu} + \sum_{ij,\mu\nu} [t_{ij,\mu\nu} c_{i,\mu}^{\dagger} c_{j,\nu} + \text{H.c.}] \quad (2)$$

where $\epsilon_{\mu,\nu}$ is the onsite energy of corresponding atom, $t_{ij,\mu\nu}$ is the hopping term, $c_{i,\mu}^{\dagger}$ is the creation operator to create an electron, i, j and μ, ν represent lattice site and atomic orbital, respectively.

For two-dimensional MoS_2 materials, the Fermi energy E_F is related to the carrier concentration n as [48, 49]

$$E_F - E_C = k_B T \times \ln(\exp^{n/N_C} - 1) \quad (3)$$

where E_C is the conduction-band minimum, k_B is the Boltzmann constant, T is the temperature and N_C is the effective density of states. $N_C = D_{2D} \times k_B T = \frac{g_v g_s m^*}{2\pi\hbar^2} \times k_B T$, where D_{2D} is the 2D density of states, g_v is the valley degeneracy, g_s is the spin degeneracy, m^* is the effective mass which can be fitted through parabolic band model and $\hbar$ is the reduced Planck constant. The relevant parameters used here are set as $g_v = 1$, $g_s = 2$, $m^* = 0.13 m_0$ (m_0 is the free-electron mass).

The tunneling current through the Schottky contact barrier can be numerically evaluated as [39, 50]

$$I = q \int_0^{\phi_d} M(E) T(E) f(E) \mathrm{d}E \quad (4)$$

where q is the electronic charge, ϕ_d is the Schottky barrier height at drain contact, $M(E)$ is the product of density of states D_{2D} and electronic average velocity v, $f(E)$ is the Fermi-Dirac distribution function and $T(E)$ is the tunneling probability which can be calculated quantum-mechanically by Wentzel-Kramers-Brillouin (WKB) approximation [50-

52]. Further, $T(E) = \exp\left(-\frac{2\sqrt{2m^*}}{\hbar} \int_0^L \sqrt{U(x) - E}\,\mathrm{d}x \right)$, where $U(x)$ is the distribution of barrier potential energy.

3. Results and Discussion

The schematic drawing of quantum tunneling transistor is shown in Fig 1(a). A single-layered armchair MoS_2 nanoribbon is placed between two electrodes. Mo-terminated edge (left boundary composed of blue spheres) is in contact with the source electrode while S-terminated edge (right boundary composed of yellow spheres) is for the drain electrode. The two red arrows indicate the edge states transport of nanoribbon from source to drain. Two-dimensional MoS_2 possesses strong piezoelectricity which is advantageous for realizing electromechanical coupling. When an external strain is imposed, a strong piezoelectric polarization field up to MV/cm could be created by the localized piezoelectric polarization charges [53]. This polarization field can be further increased while strain increases [33, 42]. Fig 1(c) demonstrates the different strain-induced barrier potential distributions of 100 nm length nanoribbon. The metal-semiconductor contact of source side is ohmic contact and the other drain side forms Schottky contact, so there exists a negligible barrier height in the left. The ohmic contact can be constructed through Schottky barrier height engineering. For example, low Schottky barrier height ~30meV has been realized in multilayer MoS_2 with scandium material contact [54] and zero Schottky barrier height can be produced for monolayer MoS_2 in contact with semimetallic bismuth [55]. As it can be seen, the barrier potential is distributed gradually except the right boundary because strain-induced piezoelectric polarization charges are mainly assembled at the zigzag edge of the nanoribbon. And the barrier height at Schottky contact increases distinctly in a larger amplitude with an increasing strain.

For a Schottky contact composed of monolayer MoS_2 with strong piezoelectric property and metal electrode, piezoelectric charges will be generated near the zigzag edge of the nanoribbon under an externally applied strain as shown in Fig 1(b) and (d). Tensile strain can induce negative piezoelectric charges near the interface which can effectively increase the Schottky barrier height and globally raise barrier potential distribution inside the

semiconductor as depicted in Fig 1(b). This phenomenon has also been studied in several previous works [12, 42, 56, 57]. The green arrows indicate the band diagram change from black dotted line to red solid line after applying tensile strain. Fig 1(d) shows the opposite situation that compressive strain can induce positive piezoelectric charges to lower the Schottky barrier height and barrier potential distribution. Thus, the charge carrier transport property through Schottky contact can be tuned by piezotronic effect depending on the strain direction.

In order to catch the edge states properties of armchair MoS_2 nanoribbon, Fig 2(a) plots the band structure of 20 nm width nanoribbon. It is noteworthy that the gapped edge modes with its edge states spectrum well-isolated from bulk states as indicated by the red lines. This specific characteristic provides direct access to study the edge states property based on low-dimensional materials. Strain-induced piezotronic effect can modulate the local Schottky barrier height and Fig 2(b) shows the barrier height as a function of applied strain. Monolayer MoS_2-metal contact usually has a barrier height based on the work function of metal contact, electron affinity of MoS_2, voltage drop at the interface and other factors [58] and 0.2 eV is set here as a reasonable value [59]. Tensile strain can increase the Schottky barrier height while compressive strain can decrease barrier height which is an effective way to regulate quantum tunneling properties.

Fig 2(c) shows the Fermi potential versus carrier concentration which can be tuned by field-effect doping technique [60-62]. The effective 2D carrier concentration reached $\sim 10^{14}$ cm^{-2} in MoS_2 [63]. High-level doping concentration $\sim 10^{13}$ cm^{-2} of monolayer MoS_2 has been studied based on dual-gated device structure [64]. Cesium carbonate and potassium are utilized as n-type doping technologies to enhance the carrier concentration in MoS_2 field-effect transistors [65, 66]. The Fermi level can be shifted with respect to conduction-band minimum through different carrier concentrations and when the concentration is set to be 0.4×10^{13} cm^{-2}, the corresponding Fermi level is at 0 eV. Tunneling probability is a key parameter for quantum tunneling transistor and Fig 2(d) shows the tunneling probability versus electronic energy for various strains. When the electronic energy is higher than barrier height, the probability is equal to 1 here. The barrier height is increased under an increasing strain thus electron needs higher energy to transport entirely.

Fig 3(a) calculates the tunneling current density for different temperatures against strain. The tunneling current density indicates an exponential decrease especially for lower temperature. The inset of Fig 3(a) shows the logarithmic scale for current density under strain. Current density is larger under a lower temperature for a lower barrier height while it becomes the reverse for higher barrier heights. It is noteworthy that strain-induced piezotronic effect can efficiently modulate the tunneling current density through modifying the barrier height and this strain control is at an exponential scale. Fig 3(b) shows the relative current sensitivity as a function of strain which is defined as $\frac{\Delta I / I_0}{\Delta s}$, where I_0 is the current without strain. This control mechanism shows an ultrahigh sensitivity which can reach over 10^3 for small compressive strain. When we further increase the strain, the sensitivity decreases due to the low tunneling current under high barrier. The systemic study of tunneling current density versus temperature and carrier concentration under strain effect by contour plot is shown in Fig 3(c) and 3(d), respectively. Upon increasing carrier concentration, the tunneling current density becomes larger. Strain reveals a remarkable control method for the performance of quantum tunneling transistor that strain can increase or decrease tunneling current density in several orders of magnitude.

Edge states transport behaviors of single-layer armchair MoS_2 nanoribbon under strain-induced piezotronic effect are further explored by Kwant Python package [67]. Fig 4(a) shows the transport conductance as a function of electronic energy under various strains for only considering strain-induced polarization and the conductance unit G_0 here is e^2/h (e is the elementary charge and h is the Plank's constant). As we can see, the edge states transport conductance is heavily decreased with an increasing strain. The inset of Fig 4(a) demonstrates the direction of strain-induced polarization electric field which is parallel to the edge states transport along armchair direction and the gradient background shows the potential distribution. The band structure, transport properties and spin polarizations of edge states in monolayer zigzag MoS_2 can be effectively controlled by piezotronic effect. The strain-induced piezoelectric field is perpendicular to the transport direction [53, 68]. For armchair MoS_2 nanoribbon, the strain-induced piezoelectric field is parallel to the edge states transport direction. Fig 4(b), (c) and (d) show the electronic density distribution of edge states transport

under 0%, 2% and 8% strain, respectively. Monolayer MoS_2-based transport is n-type [69, 70], as a result, the electronic energy is fixed at 0 eV here. The electronic behaviors provide the evidence of edge states transport as well. When there is no applied strain, electrons can pass through the nanoribbon without block as shown in Fig 4(b). Further increasing strain, the electronic transport is gradually blocked leading to the decrease of conductance as shown in Fig 4(c) and (d).

Strain-induced piezoelectric field can modify the Schottky barrier height, which is piezotronic effect on two-dimensional materials [42]. Edge states act as conducting channels [30]. The piezotronic effect can destroy the edge states in the device. Strain-induced piezoelectric field can localize the electrons at the left side, as a result, the conductance of edge states transport can be manipulated. Local strain can increase the saturation current from 3.5 pA to 17 nA in MoS_2-metal vertical devices through engineering the Schottky barrier height [40]. Both the edge states and the height of the Schottky barrier can affect the current density due to piezotronic effect. While the height of the Schottky barrier decreases by piezotronic effect, the edge states will dominate the current density. While the height of the Schottky barrier increases by piezotronic effect, both the edge states and the height of the Schottky barrier can affect the current density.

The temperature effect on transport conductance is shown in Fig 5(a) and (b). The edge states transport conductance for -0.7 eV and 0.2 eV is still $4G_0$ when the temperature increases from 0 K to 300 K as shown in Fig 5(a). Strain-induced piezotronic effect can lead to the decrease of transport conductance as well when the temperature is taken into consideration as shown in Fig 5(b). The size of nanoribbon can change the sensitivity in this quantum piezotronic transistor. Previous works reported that the tunneling current and current sensitivity depend on the length of nanoribbon. For simplicity, the width is neglected based on previous models [39, 50, 51]. The sensitivity has been calculated with various lengths of nanoribbon, as shown in Fig 5 (c). It is found that the length of nanoribbon changes the sensitivity. The sensitivity of different nanoribbon structures changes significantly due to the strain-induced piezotronic effect. The sensitivity can reach up to 10^3.

The body current can be reduced by gate voltage. Previous experiment reported that the

edge states conductance increased from 2×10^{-7} S·sq to 10^{-5} S·sq with the gate voltage varied from -20 V to 0 V [30]. The bulk states conductance was 10^{-9} S·sq. The bulk states conductance increases while gate voltage increases from 0 V to 30 V. At gate voltage of 20 V, the conductances of edge states and bulk states were 3×10^{-5} S·sq and 2×10^{-7} S·sq, respectively. The conductance of edge states is at least two orders of magnitude greater than conductance of bulk states. Therefore, the body current can be neglected in our model. Substrate pre-treatment is a typical way to improve device performance [71]. Theoretical results suggested that SiO_2 substrate might be absent for MoS_2 transistor with HfO_2 gate dielectric and an interfacial layer for best performance [72]. For example, the cantilever structure can suspend the device. ZnO nanowires can be suspended by enclosed electrodes [73]. Micro-electro-mechanical-systems (MEMS) suspension technologies may be applied in this structure [74, 75].

Fig 5(d) demonstrates two schematic diagrams of possible experimental design structure for quantum piezotronics transistor. The strain is introduced through the bottom flexible substrate. The carrier concentration in MoS_2 nanoribbon can be controlled by the applied top-gate voltage V_g [30]. MoS_2 nanoribbon is encapsulated by HfO_2 dielectric which improves carrier mobility and reduces phonon scattering [64, 76, 77]. MoS_2 nanoribbon is suspended with enclosed electrodes, as shown in the lower structure of Fig 5(d) [73].

The defects and free carrier concentration should be reduced to avoid free carriers screen effect [78]. The n-type edge states transport requires the carrier concentration of $\sim10^{12}$ cm^{-2} in our model, as shown in Fig 2(c). The free carriers screen can be effectively avoided by sulfur vacancy passivation and carrier concentration manipulation in experiments [79, 80]. DFT calculation reveals that the screen can be suppressed by contacting with metal electrodes [81]. The free carrier density decreases while temperature decreases from 320 K to 270 K [82]. The impurities in CVD growth process will be harmful to the normal operation of this piezotronic quantum tunneling device, because the free carriers from the impurities screen the strain-induced piezoelectric charges. There is a need to reduce the impurities in sample preparation [83]. In practice, it is an effective way to employ the high-quality exfoliation methods by mechanical approaches [84]. The S edge of MoS_2 nanoribbons has high stability and the S

edge has been grown experimentally without defects for MoS_2 nanoribbon [85-87].

The quantum piezotronics transistor is three-terminal device, which can be used for typical electrical circuit. The basic units for piezotronic digital circuits can be designed as shown in this work [11]. There are special strategies of the input and output interface matching circuits for electronic circuits using this device. Because this high performance quantum piezotronics transistor can operate at room temperature, this new device can even be designed directly into the typical circuits using specially designed interface circuits.

4. Conclusion

In summary, we have demonstrated a high performance piezotronic quantum tunneling transistor based on armchair MoS_2 nanoribbon, which can exploit edge states transport at room temperature. Band structure calculated from tight-binding model clearly shows the edge states spectrum. The tunneling current can be exponentially tuned by piezotronic effect. The impact of temperature and carrier concentration is discussed. The strain sensitivity can reach more than 10^3 under external strain. Besides, transport conductance and electronic density distribution under various strains are also evaluated to verify this transport behavior. This work can effectively promote the development of edge states-based applications and high performance quantum piezotronic devices at room temperature.

Credit authorship contribution statement

Minjiang Dan: Conceptualization, Methodology, Formal analysis, Data curation, Writing – original draft, Validation; **Gongwei Hu:** Conceptualization, Methodology, Formal analysis, Validation; **Lijie Li:** Writing- Reviewing and Editing; **Yan Zhang:** Conceptualization, Methodology, Supervision, Formal analysis, Writing - review & editing.

Declaration of Competing Interest

The authors declare that they have no known competing financial interests or personal relationships that could have appeared to influence the work reported in this paper.

Acknowledgments

The authors are thankful for the support from Major Project of National Natural Science

Foundation of China (Grant No. 52192612, 52192610). The authors are thankful for the support from University of Electronic Science and Technology of China (grant no. ZYGX2021YGCX001).

References

1. Wu, W. and Z.L. Wang, *Piezotronics and piezo-phototronics for adaptive electronics and optoelectronics.* Nature Reviews Materials, 2016. **1**(7).
2. Wang, Z.L., W. Wu, and C. Falconi, *Piezotronics and piezo-phototronics with third-generation semiconductors.* MRS Bulletin, 2018. **43**(12): p. 922-927.
3. Zhang, Y., et al., *Theory of piezotronics and piezo-phototronics.* MRS Bulletin, 2018. **43**(12): p. 928-935.
4. Wang, Z.L. and J. Song, *Piezoelectric nanogenerators based on zinc oxide nanowire arrays.* Science, 2006. **312**(5771): p. 242-6.
5. Wang, X., et al., *Direct-current nanogenerator driven by ultrasonic waves.* Science, 2007. **316**(5821): p. 102-5.
6. Qin, Y., X. Wang, and Z.L. Wang, *Microfibre-nanowire hybrid structure for energy scavenging.* Nature, 2008. **451**(7180): p. 809-13.
7. Zhou, J., et al., *Flexible piezotronic strain sensor.* Nano Lett, 2008. **8**(9): p. 3035-40.
8. Wang, X., et al., *Piezoelectric field effect transistor and nanoforce sensor based on a single ZnO nanowire.* Nano Lett, 2006. **6**(12): p. 2768-72.
9. Wu, W., X. Wen, and Z.L. Wang, *Taxel-addressable matrix of vertical-nanowire piezotronic transistors for active and adaptive tactile imaging.* Science, 2013. **340**(6135): p. 952-7.
10. Wu, W., Y. Wei, and Z.L. Wang, *Strain-gated piezotronic logic nanodevices.* Adv Mater, 2010. **22**(42): p. 4711-5.
11. Dan, M., et al., *High performance piezotronic logic nanodevices based on GaN/InN/GaN topological insulator.* Nano Energy, 2018. **50**: p. 544-551.
12. Zhang, Y., Y. Liu, and Z.L. Wang, *Fundamental theory of piezotronics.* Adv Mater, 2011. **23**(27): p. 3004-13.
13. Yu, Q., et al., *Highly sensitive strain sensors based on piezotronic tunneling junction.* Nat Commun, 2022. **13**(1): p. 778.
14. Niu, S., et al., *Enhanced performance of flexible ZnO nanowire based room-temperature oxygen sensors by piezotronic effect.* Adv Mater, 2013. **25**(27): p. 3701-6.
15. Yu, R., et al., *Enhanced Performance of a ZnO Nanowire-Based Self-Powered Glucose Sensor by Piezotronic Effect.* Advanced Functional Materials, 2013. **23**(47): p. 5868-5874.
16. Yu, R., C. Pan, and Z.L. Wang, *High performance of ZnO nanowire protein sensors enhanced by the piezotronic effect.* Energy & Environmental Science, 2013. **6**(2).
17. Hu, G., et al., *Piezotronic effect enhanced Schottky-contact ZnO micro/nanowire humidity sensors.* Nano Research, 2014. **7**(7): p. 1083-1091.
18. Chen, P., et al., *Large quantum-spin-Hall gap in single-layer 1T' WSe2.* Nat Commun,

2018. **9**(1): p. 2003.
19. Maurer, P.C., et al., *Room-temperature quantum bit memory exceeding one second.* Science, 2012. **336**(6086): p. 1283-6.
20. Purdy, T.P., et al., *Quantum correlations from a room-temperature optomechanical cavity.* Science, 2017. **356**(6344): p. 1265-1268.
21. Xie, C., et al., *Piezo-phototronic spin laser based on wurtzite quantum wells.* Nano Energy, 2022. **96**.
22. Chen, J.Y., et al., *Self-polarized spin-nanolasers.* Nat Nanotechnol, 2014. **9**(10): p. 845-50.
23. Zutic, I. and P.E. Faria Junior, *Semiconductor lasers: taken for a spin.* Nat Nanotechnol, 2014. **9**(10): p. 750-2.
24. Bollinger, M.V., et al., *One-dimensional metallic edge states in MoS2.* Phys Rev Lett, 2001. **87**(19): p. 196803.
25. Helveg, S., et al., *Atomic-scale structure of single-layer MoS2 nanoclusters.* Phys Rev Lett, 2000. **84**(5): p. 951-4.
26. Bollinger, M.V., K.W. Jacobsen, and J.K. Nørskov, *Atomic and electronic structure ofMoS2nanoparticles.* Physical Review B, 2003. **67**(8).
27. Yuan, N.F., K.F. Mak, and K.T. Law, *Possible topological superconducting phases of MoS2.* Phys Rev Lett, 2014. **113**(9): p. 097001.
28. Chu, R.-L., et al., *Spin-orbit-coupled quantum wires and Majorana fermions on zigzag edges of monolayer transition-metal dichalcogenides.* Physical Review B, 2014. **89**(15).
29. Woodward, R.I., et al., *Tunable Q-switched fiber laser based on saturable edge-state absorption in few-layer molybdenum disulfide (MoS(2)).* Opt Express, 2014. **22**(25): p. 31113-22.
30. Wu, D., et al., *Uncovering edge states and electrical inhomogeneity in MoS2 field-effect transistors.* Proc Natl Acad Sci U S A, 2016. **113**(31): p. 8583-8.
31. Radisavljevic, B., et al., *Single-layer MoS2 transistors.* Nat Nanotechnol, 2011. **6**(3): p. 147-50.
32. Rai, A., et al., *Progress in Contact, Doping and Mobility Engineering of MoS2: An Atomically Thin 2D Semiconductor.* Crystals, 2018. **8**(8).
33. Bertolazzi, S., J. Brivio, and A. Kis, *Stretching and breaking of ultrathin MoS2.* ACS Nano, 2011. **5**(12): p. 9703-9.
34. van der Zande, A. and J. Hone, *Inspired by strain.* Nature Photonics, 2012. **6**(12): p. 804-806.
35. Wang, Q.H., et al., *Electronics and optoelectronics of two-dimensional transition metal dichalcogenides.* Nat Nanotechnol, 2012. **7**(11): p. 699-712.
36. Manzeli, S., et al., *2D transition metal dichalcogenides.* Nature Reviews Materials, 2017. **2**(8).
37. Sarkar, D., et al., *A subthermionic tunnel field-effect transistor with an atomically thin channel.* Nature, 2015. **526**(7571): p. 91-5.
38. Lan, Y.W., et al., *Atomic-Monolayer MoS2 Band-to-Band Tunneling Field-Effect Transistor.* Small, 2016. **12**(41): p. 5676-5683.
39. Das, S., et al., *Toward low-power electronics: tunneling phenomena in transition*

metal dichalcogenides. ACS Nano, 2014. **8**(2): p. 1681-9.
40. Quereda, J., et al., *Strain engineering of Schottky barriers in single- and few-layer MoS2 vertical devices.* 2D Materials, 2017. **4**(2).
41. Duerloo, K.-A.N., M.T. Ong, and E.J. Reed, *Intrinsic Piezoelectricity in Two-Dimensional Materials.* The Journal of Physical Chemistry Letters, 2012. **3**(19): p. 2871-2876.
42. Wu, W., et al., *Piezoelectricity of single-atomic-layer MoS2 for energy conversion and piezotronics.* Nature, 2014. **514**(7523): p. 470-4.
43. Bussy, A., G. Pizzi, and M. Gibertini, *Strain-induced polar discontinuities in two-dimensional materials from combined first-principles and Schrödinger-Poisson simulations.* Physical Review B, 2017. **96**(16).
44. Zhang, J., et al., *Band alignment of two-dimensional lateral heterostructures.* 2D Materials, 2016. **4**(1).
45. Ong, M.T., K.-A.N. Duerloo, and E.J. Reed, *The Effect of Hydrogen and Fluorine Coadsorption on the Piezoelectric Properties of Graphene.* The Journal of Physical Chemistry C, 2013. **117**(7): p. 3615-3620.
46. Khoeini, F., K. Shakouri, and F.M. Peeters, *Peculiar half-metallic state in zigzag nanoribbons ofMoS2: Spin filtering.* Physical Review B, 2016. **94**(12).
47. Rostami, H., R. Asgari, and F. Guinea, *Edge modes in zigzag and armchair ribbons of monolayer MoS2.* J Phys Condens Matter, 2016. **28**(49): p. 495001.
48. Ng, H.K., D. Chi, and K. Hippalgaonkar, *Effect of dimensionality on thermoelectric powerfactor of molybdenum disulfide.* Journal of Applied Physics, 2017. **121**(20).
49. Hippalgaonkar, K., et al., *High thermoelectric power factor in two-dimensional crystals ofMoS2.* Physical Review B, 2017. **95**(11).
50. Myoung, N., et al., *Large current modulation and spin-dependent tunneling of vertical graphene/MoS2 heterostructures.* ACS Nano, 2013. **7**(8): p. 7021-7.
51. Lingaparthi, R., et al., *Surface related tunneling leakage in β-Ga2O3 (001) vertical Schottky barrier diodes.* Applied Physics Express, 2019. **12**(7).
52. Osvald, J., *Numerical simulation of tunneling current in GaN Schottky diodes.* Journal of Applied Physics, 2007. **101**(10).
53. Wang, K., et al., *Polarization-Driven Edge-State Transport in Transition-Metal Dichalcogenides.* Physical Review Applied, 2020. **13**(5).
54. Das, S., et al., *High performance multilayer MoS2 transistors with scandium contacts.* Nano Lett, 2013. **13**(1): p. 100-5.
55. Shen, P.C., et al., *Ultralow contact resistance between semimetal and monolayer semiconductors.* Nature, 2021. **593**(7858): p. 211-217.
56. Zhou, J., et al., *Piezoelectric-potential-controlled polarity-reversible Schottky diodes and switches of ZnO wires.* Nano Lett, 2008. **8**(11): p. 3973-7.
57. Gao, Z., et al., *Effects of piezoelectric potential on the transport characteristics of metal-ZnO nanowire-metal field effect transistor.* J Appl Phys, 2009. **105**(11): p. 113707.
58. Tung, R.T., *Chemical bonding and fermi level pinning at metal-semiconductor interfaces.* Phys Rev Lett, 2000. **84**(26 Pt 1): p. 6078-81.
59. Pan, Y., et al., *Reexamination of the Schottky Barrier Heights in Monolayer MoS2*

Field-Effect Transistors. ACS Applied Nano Materials, 2019. **2**(8): p. 4717-4726.

60. Brumme, T., M. Calandra, and F. Mauri, *First-principles theory of field-effect doping in transition-metal dichalcogenides: Structural properties, electronic structure, Hall coefficient, and electrical conductivity.* Physical Review B, 2015. **91**(15).
61. Tong, X., et al., *Advances in MoS2-Based Field Effect Transistors (FETs).* Nanomicro Lett, 2015. **7**(3): p. 203-218.
62. Schmidt, H., F. Giustiniano, and G. Eda, *Electronic transport properties of transition metal dichalcogenide field-effect devices: surface and interface effects.* Chem Soc Rev, 2015. **44**(21): p. 7715-36.
63. Ye, J.T., et al., *Superconducting dome in a gate-tuned band insulator.* Science, 2012. **338**(6111): p. 1193-6.
64. Radisavljevic, B. and A. Kis, *Mobility engineering and a metal-insulator transition in monolayer MoS(2).* Nat Mater, 2013. **12**(9): p. 815-20.
65. Lin, J.D., et al., *Electron-doping-enhanced trion formation in monolayer molybdenum disulfide functionalized with cesium carbonate.* ACS Nano, 2014. **8**(5): p. 5323-9.
66. Fang, H., et al., *Degenerate n-doping of few-layer transition metal dichalcogenides by potassium.* Nano Lett, 2013. **13**(5): p. 1991-5.
67. Groth, C.W., et al., *Kwant: a software package for quantum transport.* New Journal of Physics, 2014. **16**(6).
68. Yan, X.F., et al., *High performance piezotronic spin transistors using molybdenum disulfide nanoribbon.* Nano Energy, 2020. **75**.
69. Baugher, B.W., et al., *Intrinsic electronic transport properties of high-quality monolayer and bilayer MoS2.* Nano Lett, 2013. **13**(9): p. 4212-6.
70. Kaasbjerg, K., K.S. Thygesen, and K.W. Jacobsen, *Phonon-limited mobility inn-type single-layer MoS2from first principles.* Physical Review B, 2012. **85**(11).
71. Yin, H., et al., *Substrate effects on the CVD growth of MoS2 and WS2.* Journal of Materials Science, 2019. **55**(3): p. 990-996.
72. Zeng, L., et al., *Remote phonon and impurity screening effect of substrate and gate dielectric on electron dynamics in single layer MoS2.* Applied Physics Letters, 2013. **103**(11).
73. Zhang, Y., et al., *Effects of piezopotential spatial distribution on local contact dictated transport property of ZnO micro/nanowires.* Applied Physics Letters, 2010. **97**(3).
74. Lysenko, I.E., D.V. Naumenko, and O.A. Ezhova, *Design and simulation high aspect ratio torsion suspension of MEMS z-axis accelerometer.* Journal of Physics: Conference Series, 2020. **1695**(1).
75. Lee, S.-H., et al. *A low-power oven-controlled vacuum package technology for high-performance MEMS.* in *2009 IEEE 22nd International Conference on Micro Electro Mechanical Systems*. 2009. IEEE.
76. Amani, M., et al., *Growth-substrate induced performance degradation in chemically synthesized monolayer MoS2 field effect transistors.* Applied Physics Letters, 2014. **104**(20).
77. Fuhrer, M.S. and J. Hone, *Measurement of mobility in dual-gated MoS(2) transistors.* Nat Nanotechnol, 2013. **8**(3): p. 146-7.

78. Lin, P., et al., *Piezo-Phototronic Effect for Enhanced Flexible MoS2/WSe2 van der Waals Photodiodes*. Advanced Functional Materials, 2018. **28**(35).
79. Han, S.A., et al., *Point-Defect-Passivated MoS2 Nanosheet-Based High Performance Piezoelectric Nanogenerator.* Adv Mater, 2018. **30**(21): p. e1800342.
80. Lin, P., et al., *Defect repair for enhanced piezo-phototronic MoS2 flexible phototransistors.* Journal of Materials Chemistry C, 2019. **7**(46): p. 14731-14738.
81. Liu, W., et al., *Density functional studies on edge-contacted single-layer MoS2 piezotronic transistors.* Applied Physics Letters, 2015. **107**(8).
82. Sohn, A., et al., *Temperature-dependent piezotronic effect of MoS2 monolayer.* Nano Energy, 2019. **58**: p. 811-816.
83. Wang, W., et al., *Defect Passivation and Photoluminescence Enhancement of Monolayer MoS2 Crystals through Sodium Halide-Assisted Chemical Vapor Deposition Growth.* ACS Appl Mater Interfaces, 2020. **12**(8): p. 9563-9571.
84. Cui, C., et al., *Two-dimensional materials with piezoelectric and ferroelectric functionalities.* npj 2D Materials and Applications, 2018. **2**(1).
85. Li, Y., et al., *MoS2 nanoribbons: high stability and unusual electronic and magnetic properties.* J Am Chem Soc, 2008. **130**(49): p. 16739-44.
86. Wang, Z., et al., *Mixed low-dimensional nanomaterial: 2D ultranarrow MoS2 inorganic nanoribbons encapsulated in quasi-1D carbon nanotubes.* J Am Chem Soc, 2010. **132**(39): p. 13840-7.
87. Pan, H. and Y.-W. Zhang, *Edge-dependent structural, electronic and magnetic properties of MoS2 nanoribbons.* Journal of Materials Chemistry, 2012. **22**(15).

Figure caption

Figure 1 (a) Quantum tunneling transistor based on armchair MoS_2 nanoribbon. The left boundary atoms are Mo (blue spheres) while S (yellow spheres) for right boundary atoms and the red arrows indicate the edge states transport from source to drain. (b) Tensile strain-induced piezotronic effect on the schematic band diagram. (c) Strain-induced barrier potential distribution from source ohmic contact to drain Schottky contact for 100 nm nanoribbon length. (d) Compressive strain-induced piezotronic effect on the schematic band diagram. The red solid line and black dotted line represent the band diagram considering and not considering polarization charges, respectively.

Figure 2 (a) Band structure of armchair MoS_2 nanoribbon for 20 nm width. (b) Schottky barrier height as a function of applied strain. (c) Fermi potential against carrier concentration. (d) Tunneling probability versus electronic energy under different strains.

Figure 3 (a) Tunneling current density for different temperatures versus strain (carrier concentration is 10^{13} cm^{-2}). The inset shows the logarithmic scale. (b) Relative current sensitivity as a function of strain under different temperatures. Contour plot of tunneling current density versus strain and (c) temperature and (d) carrier concentration.

Figure 4 (a) Conductance of armchair MoS_2 nanoribbon versus electronic energy under various strains for only considering strain-induced polarization at 0 K. The inset indicates the direction of strain-induced polarization field and the gradient background shows the electric potential distribution. The width is 20 nm and the length is 100 nm. Electronic density distribution of edge states transport under (b) 0% strain, (c) 2% strain, (d) 8% strain. The electronic energy is fixed at 0 eV. The nanoribbon is of 4 nm width and 6 nm length for an intuitive presentation.

Figure 5 Conductance of armchair MoS_2 nanoribbon versus electronic energy under different temperatures for (a) 0% strain and (b) 2% strain. (c) Relative current sensitivity versus strain for different nanoribbon lengths (carrier concentration is 10^{13} cm^{-2} and the temperature is 300

K). (d) Schematic diagrams of possible experimental design structure for quantum piezotronics transistor.

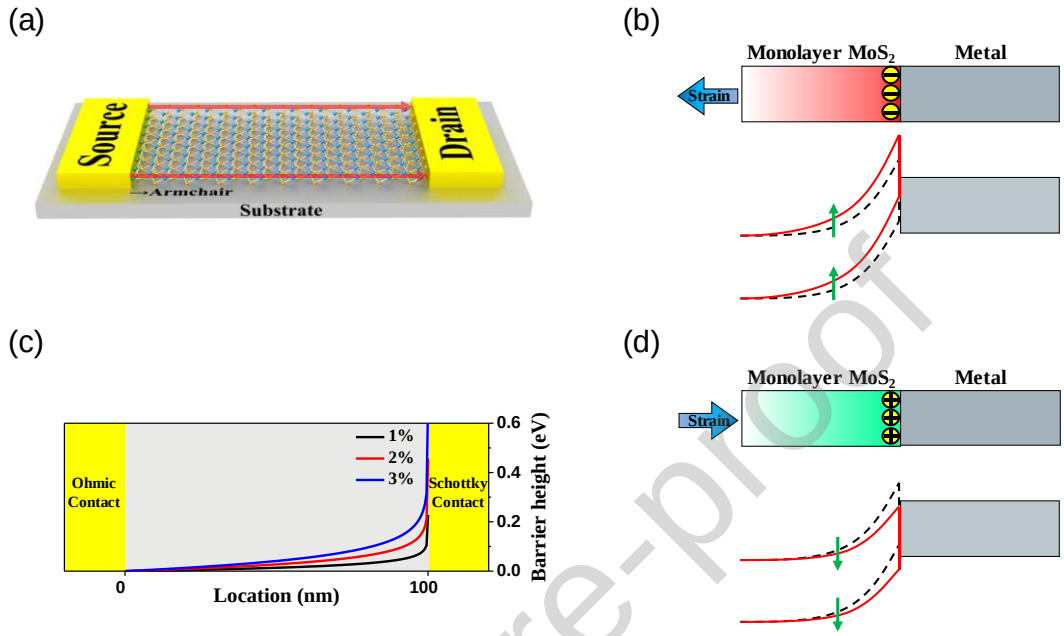

Figure 1

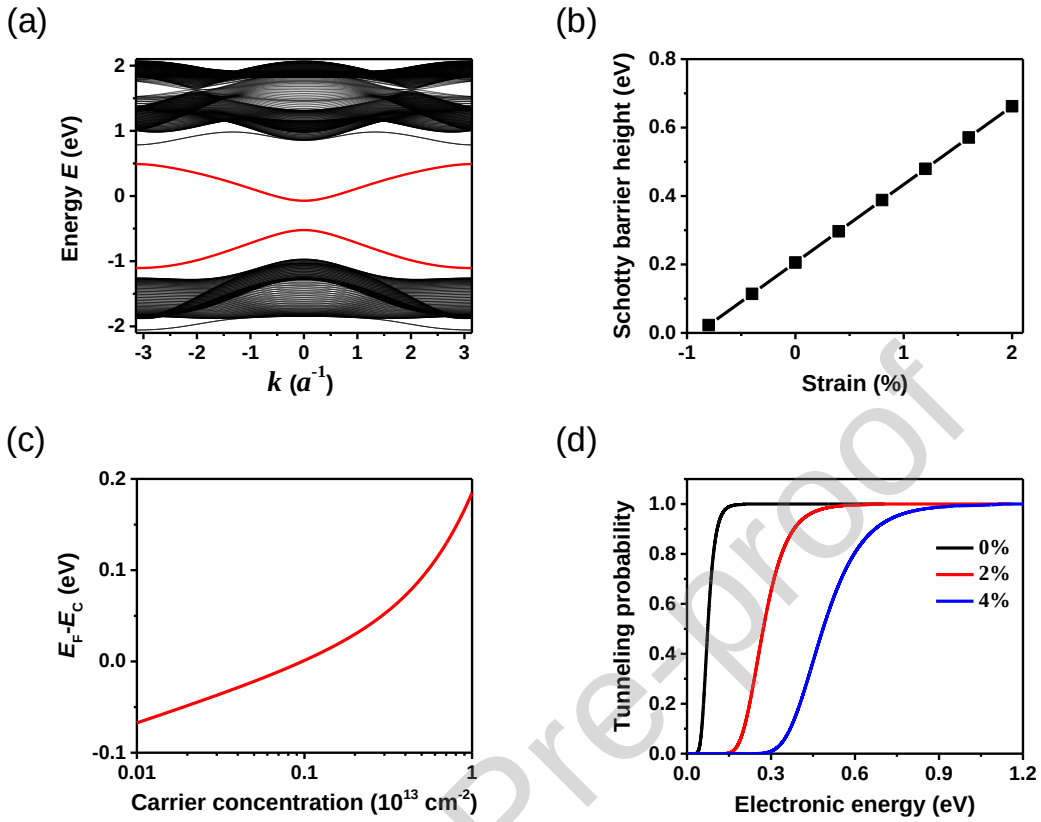

Figure 2

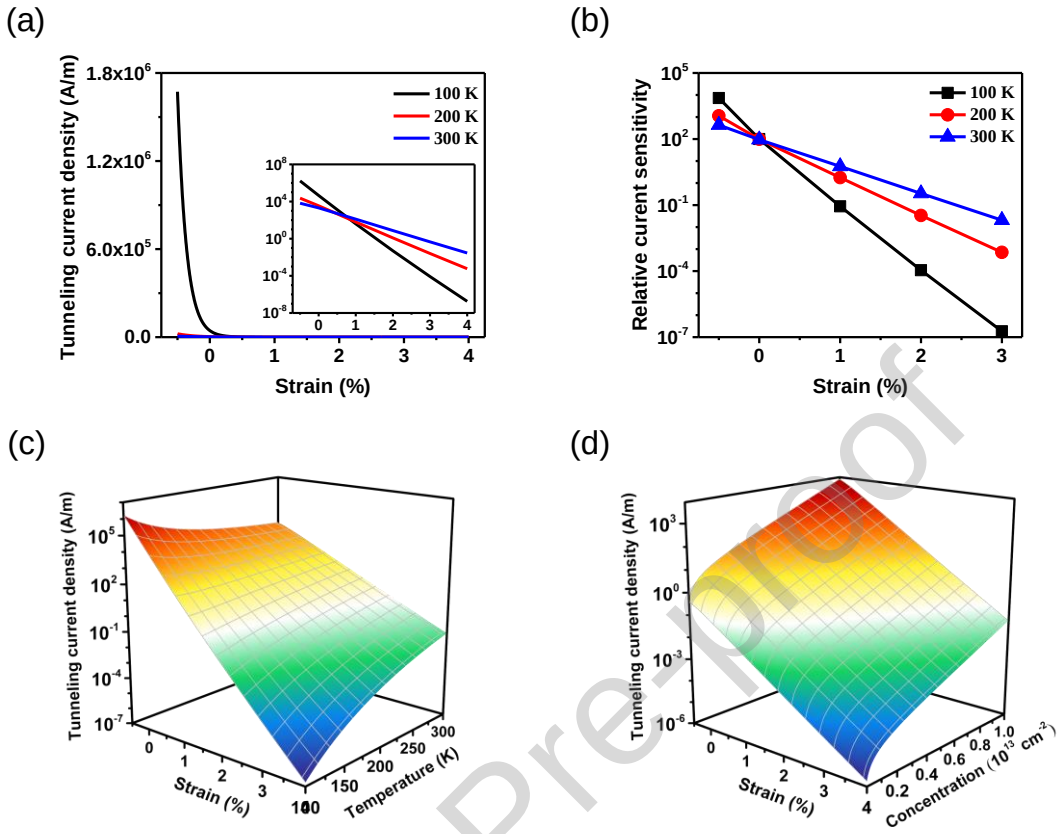

Figure 3

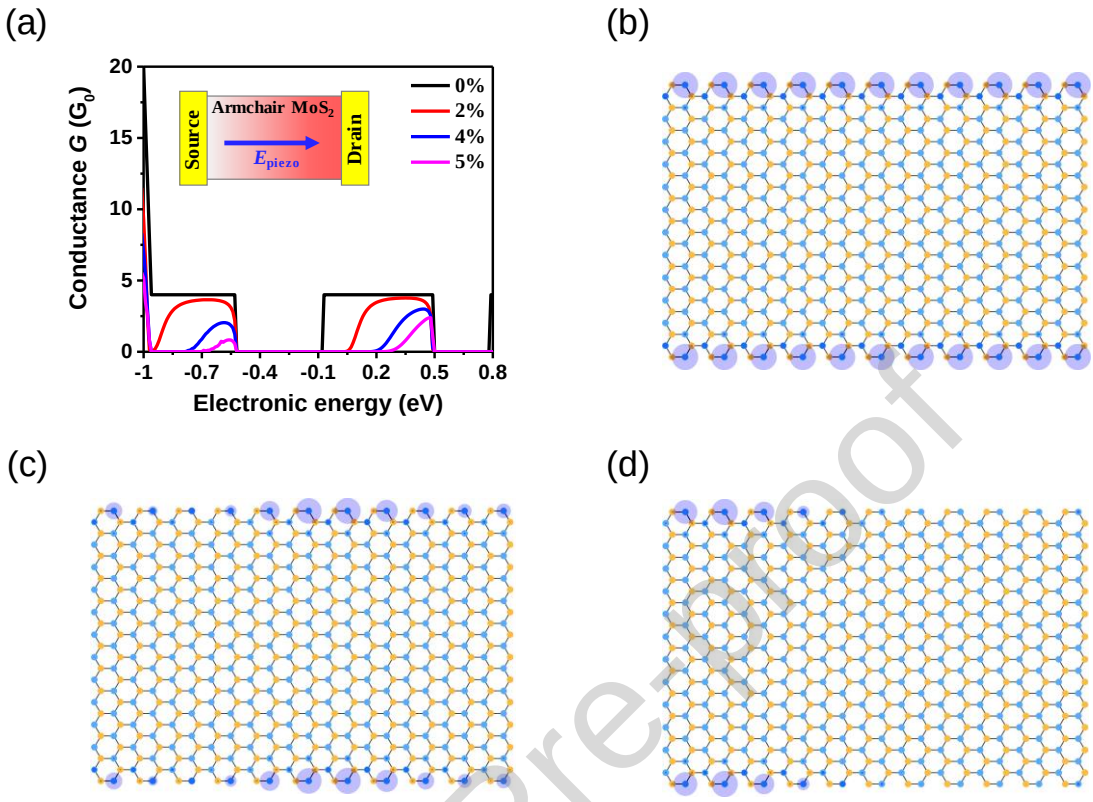

Figure 4

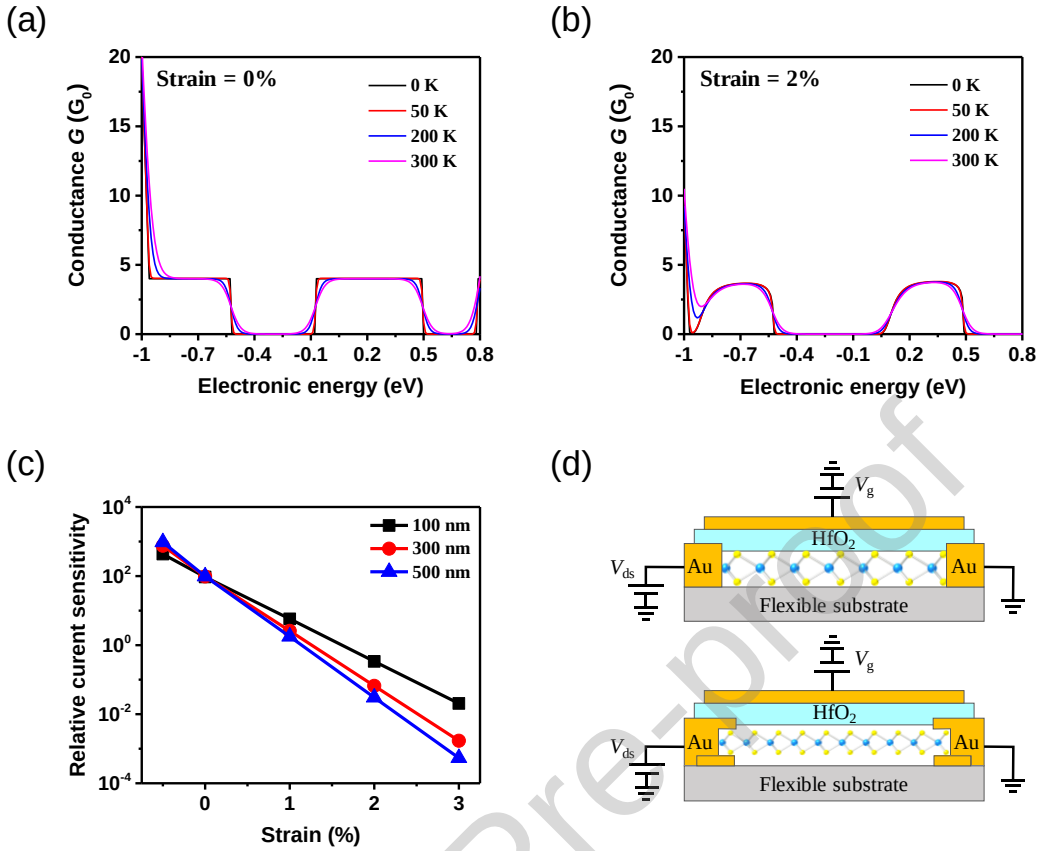

Figure 5

Credit authorship contribution statement

Minjiang Dan: Conceptualization, Methodology, Formal analysis, Data curation, Writing – original draft, Validation; **Gongwei Hu:** Conceptualization, Methodology, Formal analysis, Validation; **Lijie Li:** Writing- Reviewing and Editing; **Yan Zhang:** Conceptualization, Methodology, Supervision, Formal analysis, Writing - review & editing.

Declaration of interests

☒ The authors declare that they have no known competing financial interests or personal relationships that could have appeared to influence the work reported in this paper.

☐The authors declare the following financial interests/personal relationships which may be considered as potential competing interests:

Graphical abstract:

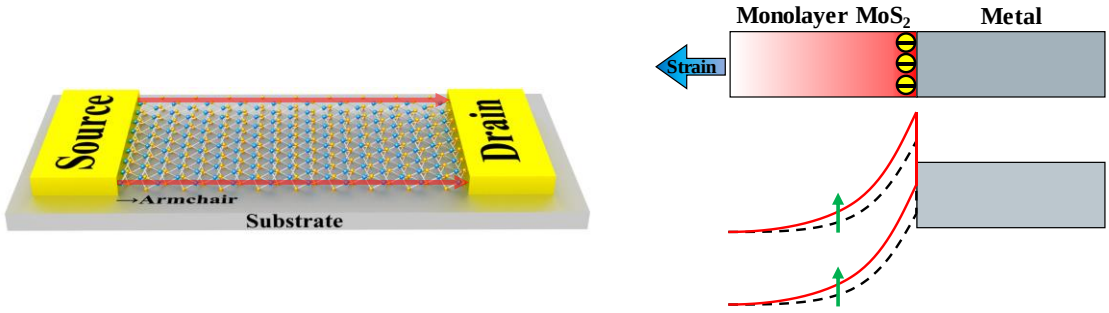

Edge states-based quantum piezotronic tunneling transistor using an armchair MoS_2 nanoribbon is constructed. The tunneling current can be exponentially controlled by the piezotronic effect, which exhibits ultrahigh sensitivity over 10^3. The edge states transport properties are further studied by the transport conductance and electronic density distribution under various strains.

Highlights:

- Quantum tunneling transistor based on armchair MoS_2 nanoribbon is innovatively designed to exploit edge states transport.
- Piezotronic effect can exponentially tune the tunneling current through adjusting the Schottky barrier and the sensitivity can reach over 10^3.
- Edge states transport behaviors are further investigated by simulating the conductance and electronic density distribution under different strains.
- This study provides constructive design methods for realizing edge states-based electronic devices and high performance room temperature quantum piezotronics devices.